Acta Pharmaceutica Sinica B 2025;15(6):3305−3320

Chinese Pharmaceutical Association
Institute of Materia Medica, Chinese Academy of Medical Sciences

Acta Pharmaceutica Sinica B

www.elsevier.com/locate/apsb
www.sciencedirect.com

ORIGINAL ARTICLE

Pitavastatin-loaded procyanidins self-assembled nanoparticles alleviate advanced atherosclerosis *via* modulating macrophage efferocytosis and cholesterol efflux

Yizhou Wu[a,†], Hongyan Zhou[b,†], Hao Liu[c,†], Jiayao Hu[a], Yue Sun[a,d], Wei Yan[e], Chunyi Tong[a], Ying Kong[c,*], Bin Liu[a,d,*]

[a]*College of Biology, Hunan University, Changsha 410082, China*
[b]*Precision Pharmacy & Drug Development Center, Department of Pharmacy, Second Affiliated Hospital, Air Force Medical University, Xi'an 710038, China*
[c]*Department of Rehabilitation, The Second Xiangya Hospital, Central South University, Changsha 410011, China*
[d]*NHC Key Laboratory of Metabolic Cardiovascular Diseases Research, Department of Physiology and Pathophysiology, School of Basic Medical Sciences, Ningxia Medical University, Yinchuan 750004, China*
[e]*Key Laboratory of Medical Electrophysiology of Ministry of Education and Medical Electrophysiological Key Laboratory of Sichuan Province, Institute of Cardiovascular Research, Southwest Medical University, Luzhou 646000, China*

Received 6 January 2024; received in revised form 18 April 2024; accepted 7 August 2024

KEY WORDS

Advanced atherosclerosis;
Procyanidins;
Pitavastatin;
Efferocytosis;
Macrophage lipophagy;
Self-assembled nanoparticles

Abstract Advanced atherosclerosis is the major global cause of death, as featured by the aggregation of apoptotic cells (ACs) in necrotic cores. The defective efferocytosis and dysfunctional cholesterol efflux of macrophages are the main reasons for forming necrotic cores in advanced atherosclerosis. In this study, we constructed self-assembled procyanidins (PC) NPs for loading pitavastatin (Pita). The designed HA@PC@Pita NPs with hyaluronic acid (HA) modification combined the advantages of efferocytosis restoration of Pita and cholesterol efflux enhancement of PC. *In vitro* assay indicated that HA@PC@Pita NPs could induce M1/M2 repolarization and upregulate ERK5/Mertk expression to restore efferocytosis of macrophages. Simultaneously, HA@PC@Pita NPs notably promoted cholesterol efflux by promoting macrophage lipophagy, a selective autophagy of lipid droplets. *In vivo* study showed

*Corresponding authors.
E-mail addresses: binliu2001@hotmail.com (Bin Liu), kongying1502@csu.edu.cn (Ying Kong).
†These authors made equal contributions to this work.

Peer review under the responsibility of Chinese Pharmaceutical Association and Institute of Materia Medica, Chinese Academy of Medical Sciences.

https://doi.org/10.1016/j.apsb.2024.08.006

that HA@PC@Pita NPs cleared necrotic core and enhanced plaque stability in the *ApoE*$^{-/-}$ mice model with advanced atherosclerosis. Taken together, this study demonstrated the potential of HA@PC@Pita NPs for the treatment of advanced atherosclerosis.

1. Introduction

Cardiovascular disease caused by atherosclerosis represents a chronic pathological condition affecting the large and medium-sized arterial systemically[1]. The necrotic core, a hallmark of advanced atherosclerosis plaques, develops through the progressive aggregation of apoptotic cells (ACs) surrounded by cholesterol-rich foam cells, leading to the formation of vulnerable plaques and plaque disruption[2]. Efferocytosis, a conserved clearance mechanism in atherosclerotic lesions, plays a critical role in removing ACs prior to the formation of foam cells-enriched necrotic core[3]. However, the substantial cholesterol accumulation in macrophages following ACs phagocytosis impairs macrophage cholesterol efflux function, creating a vicious cycle of defective efferocytosis and progressive expansion of atherosclerotic lesions[4]. This pathophysiological cascade underscores the therapeutic potential of simultaneously restoring defective efferocytosis and promoting cholesterol efflux of macrophages as a promising strategy to mitigate progression in advanced atherosclerosis.

Atherosclerosis-related molecular mechanisms governing efferocytosis have demonstrated that exposure of the "eat-me" signal on the ACs surface can attract macrophages to efficiently engulf and clear these cells[5]. Heo et al.[6] further reported that the activation of extracellular-signal-regulated kinase 5 (ERK5) enhanced efferocytic capacity by upregulating Mertk (Mer tyrosine kinase about "eat-me" signaling), a critical receptor mediating "eat-me" signal recognition, thereby promoting macrophage-mediated phagocytic clearance. Pitavastatin (Pita) is one kind of the statin's lipid-lowering class of drugs[7]. Intriguingly, Emerging evidences indicated that Pita could skew pro-inflammatory M1 phenotype toward the pro-efferocytosis M2 macrophages in the plaque *via* activating ERK5, thereby enhancing ACs clearance[6,8]. Complementarily, polyphenol flavonoid member procyanidins (PC) was reported to inhibit macrophage foaming mainly through up-regulating cholesterol efflux-related proteins ABCA1/G1. Notably, cholesterol efflux is mechanistically linked to lipophagy, a selective autophagy[9], wherein lipid droplets are metabolized *via* lysosomal degradation orchestrated by lipophagy-specific regulators and core autophagy machinery[10]. Since lipid-laden foam cells and unresolved ACs synergistically drive necrotic core expansion in advanced plaques, it is reasonable to suppose that the combination of Pita and PC, represents a mechanistically grounded strategy to alleviate advanced by simultaneously restoring efferocytosis and promoting cholesterol efflux.

However, the simultaneous delivery of Pita and PC to activated macrophages in plaques while maintaining therapeutic functions remains a significant challenge[11]. Recent advances in nanotechnology have enabled the development of dual-drug delivery systems targeting plaques for atherosclerosis treatment with promising efficacy[12]. Nevertheless, these approaches exhibit notable limitations such as excessive carrier requirement, structural complexity, poor drug release control, and prolonged treatment duration, etc[13]. Emerging carrier-free strategies utilizing self-assembled nanoparticles showed potential to improve drug treatment efficiency as well as drug loading[14]. For example, Tian et al.[15] demonstrated that Epigallocatechin (EGCG) self-assembled nanoparticles achieved comparable ROS scavenging capability at half the dosage of free EGCG. Notably, Chen et al.[16] developed EGCG-based self-assembled nanoparticles with 98% encapsulation efficiency for β-cyclodextrin in hyperlipidemia management. In addition, the 9-fluoromethoxy carbon motif group, which shares $\pi-\pi$ conjugation characteristics with EGCG's phenolic structure, was found to confer self-assembly capability when conjugated with PEG[17]. Given the structural similarity between PC's polyphenolic flavonoids framework and EGCG's core structure[18], PC may spontaneously form self-assembled nanoparticles suitable for Pita delivery to atherosclerotic plaque.

In this study, we engineered self-assembly PC NPs co-loaded with Pita (PC@Pita NPs) to synergistically restore efferocytosis and enhance cholesterol efflux. The functionalized PC NPs were prepared *via* polyphenolic condensation and benzoxazine reaction[18]. At first, the self-assembly of PC forms linear polyphenol oligomeric molecules under appropriate conditions[19]. The concentration increase of oligomeric molecules leads to gradually aggregate to form hollow polyphenol NPs through hydrogen bonding and $\pi-\pi$ stacking interaction[20]. Afterwards, solvent-mediated depolymerization-reassembly cycles enabled high-efficiency Pita encapsulation and reassembly of PC NPs through the interaction between the phenolic hydroxyl groups of PC and the carboxyl moiety of Pita[21]. Then, hyaluronic acid (HA) was conjugated to the surface of the PC@Pita NPs to endow targeting ability to activated macrophages in plaques by interacting with CD44 highly expressed on the activated macrophages[22]. Therefore, HA@PC@Pita NPs can targetly co-deliver Pita and PC to activated macrophages in plaques to alleviate advanced atherosclerosis *via* simultaneously restoring efferocytosis and promoting cholesterol efflux (Scheme 1).

2. Materials and methods

2.1. Reagents and materials

Procyanidins (PC) were bought from Solarbio (Beijing, China). Pitavastatin (Pita) was provided by Aladdin (Shanghai, China). Hyaluronic acid (HA) was supplied by Dalian Meilun (Dalian, China). DAPI, LysoTracker and Oil Red O (ORO) were obtained from Sigma−Aldrich (MO, USA). ELISA kits were obtained by

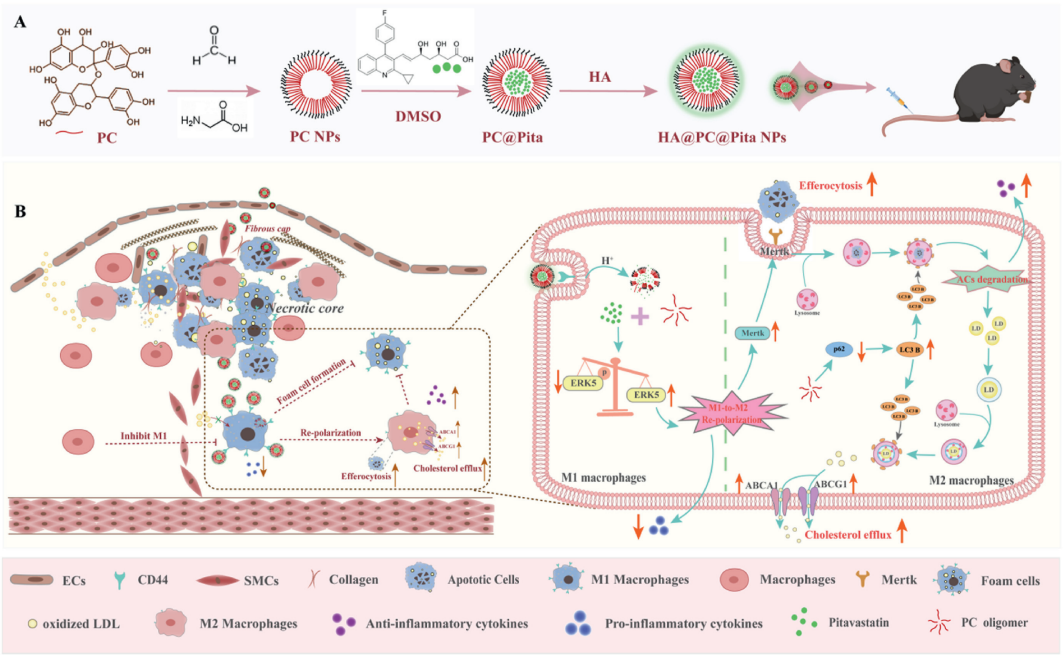

Scheme 1 Schematic preparation of HA@PC@Pita NPs and the strategy for advanced atherosclerosis treatment. (A) Preparation scheme of HA@PC@Pita NPs. (B) HA@PC@Pita NPs alleviate advanced atherosclerosis by restoring efferocytosis and promoting cholesterol efflux.

Neobioscience Biotechnology Co., Ltd. (China). Hochest 33342, and TUNEL kit was purchased from Yeasen biotech Co., Ltd. (Shanghai, China). 3-Methyladenine (3-MA) was purchased from MedChemExpress (Shanghai).

Primary antibodies: anti-CD80, anti-CD206, anti-p62, anti-LC3 B, anti-p-ERK5, anti-ABCA1, anti-ABCG1, and anti-GAPDH were supplied by Proteintech (Wuhan, China). Anti-ERK5 and anti-Mertk were obtained from Abcam (Britain).

2.2. *Preparation of nanoparticles*

2.2.1. *Preparation of PC NPs*

First, 10 μL HCHO (final concentration, 37%) was added into a red-brown solution containing 10 mg PC in 4 mL ddH_2O (final concentration, 2.5 mg/mL), and reacted at 800 rpm (Eppendorf, Hamburg, Germany) for 5 min in the dark. Then, 0.8 mL ddH_2O containing 8 mg glycine (Gly) was added into the solution and stirred at 800 rpm for 2 h. Finally, the obtained PC NPs were dialyzed in a 3.5 kDa dialysis bag for 6 h, and the internal solution was stored at −20 °C after freeze-drying.

2.2.2. *Preparation of PC@Pita NPs*

3 mg PC NPs were dissolved in 100 μL DMSO and sonicated for 2 min (40 W), and then added 10 μL Pita (final concentration, 0.2 mg/mL) to the solution. After ultrasound at 40 W for 2 min, the resulting solution was added into 1 mL 1% PVA solution and stirred at 800 rpm for 2 min. After ultrasound for 5 min (40 W), the sample was stirred for 24 h. Ultimately, the obtained PC@Pita NPs were dialyzed in a 1 kDa dialysis bag for 6 h, and the internal solution was stored at −20 °C after freeze-drying.

2.2.3. *Formulation of HA@PC@Pita NPs*

PC@Pita NPs was synthesized according to the method in Section 2.2.2. 5 μL HA (final concentration, 5 mg/mL) was mixed with 1 mL PC@Pita NPs solution and stirred for 12 h. Ultimately, the obtained HA@PC@Pita NPs were dialyzed in the 1 kDa dialysis bag for 6 h and stored at −20 °C after freeze-drying.

2.2.4. *Physicochemical characterization of prepared NPs*

Malvern Dynamic light scattering (DLS) was used to characterize the ζ-potential and size in different samples. The surface shape and morphology characterization of the NPs was imaged by transmission electron microscope (TEM). The encapsulation efficiency (EE) and drug loading (LE) were evaluated by UV−Vis absorption spectrum. Fourier transform infrared spectroscopy (FT-IR) was adopted to analyze the chemical bonds in the nanoparticles. EE and LE were calculated using the following equation:

$$\text{EE}\ (\%) = \text{Amount of Pita loaded in PC NPs/Initial Pita amount} \times 100 \quad (1)$$

$$\text{LE}\ (\%) = \text{Amount of Pita loaded in PC NPs/Amount of PC NPs} \times 100 \quad (2)$$

$$\text{Cumulative drug release}\ (\%) = M_t/M_0 \times 100 \quad (3)$$

where M_t is the amount of drug released, M_0 is the initial amount of drug in the nanomaterials. The experiment was repeated three times.

2.3. *In vitro characterization*

2.3.1. *Cell culture*

DMEM (Gibco) medium supplementing with 10% fetal calf serum and 1% penicillin−streptomycin solution was utilized to culture mononuclear leukemia cell line (RAW264.7), human umbilical vein endothelial cell line (HUVEC), vascular smooth muscle cell line (VSMC), human liver cell line (HL7702), and rat cardiac myoblast (H9C2) in a 5% CO_2 incubator at 37 °C. 1640 medium

containing 10% fetal calf serum (10%FBS, Gibco) and 1% penicillin−streptomycin solution was used to culture jurkat cells. Activated macrophages were obtained by incubating with lipopolysaccharide (LPS, 100 ng/mL, Sigma−Aldrich).

2.3.2. Cellular target ability of HA@PC@Pita NPs

The target ability assay of HA@PC@Pita NPs to activated macrophages was performed in 12-well plated. Initially, Ce6-labeled (5 μg/mL) NPs were mixed with the activated macrophages for 4 h. After washing cells with PBS for three times, Hochest33342 was used to stain the nucleus. Ultimately, cells were observed and imaged under CLSM (Olympus, FV1200).

2.3.3. Assessment of immune escape ability of HA@PC@Pita NPs

Macrophages with a cell density of 10^6 were cultivated in 12 well plates for 24 h Ce6-labeled (the Ce6 concentration was 5 μg/mL) NPs were then added into the plates at 2, 4, and 6 h. After using DAPI to stain the nucleus for 30 min, the immune escape ability was observed and imaged under CLSM (Olympus, FV1200).

2.3.4. Transwell assay

24-well plates were seeded with macrophages and the HUVECs was seeded in the upper chamber for 24 h, 100 ng/mL LPS was used to stimulate cells. PC@Ce6 NPs and HA@PC@Ce6 NPs (the Ce6 concentration was 5 μg/mL) were added into activated HUVECs for 4 h. DAPI was used to stain the nucleus for 30 min, the permeability of NPs was observed under CLSM (Olympus, FV1200).

2.4. Mechanisms of anti-atherosclerosis

2.4.1. Ox-LDL uptake and Oil Red O staining in macrophages

100 ng/mL LPS was used to stimulate macrophages in the 24-well plates for 24 h to form activated macrophages. Then, the cells were pretreated with HA@PC@Pita NPs for 2 h and co-cultured with oxLDL (80 μg/mL) for 48 h. Lipid droplets stained with 0.3% ORO in activated macrophages were imaged using inverted fluorescence microscope (Olympus, IX-73).

2.4.2. Immunofluorescence of M1/M2-type repolarization

Macrophages were cultured in the 24-well plates at the density of 1.5×10^5 cells per well with cover slip and activated with 500 ng/mL LPS stimulation for 24 h. Subsequently, activated macrophages were incubated with NPs overnight and fixed with 4% paraformaldehyde for 30 min. Then, cells were incubated with the primary antibodies at 4 °C overnight against CD80 (1:200) and CD206 (1:250), and fluorescent-labelled secondary antibody was added for 4 h. After being stained with DAPI for 30 min, the fluorescence images were photographed by Nikon (Ti-E + A1 MP, Japan) confocal microscope.

2.4.3. In vitro efferocytosis assay

RAW264.7 cells plated in the 24-well plates (1.5×10^5 cells/well) were stimulated with LPS (100 ng/mL) overnight and then incubated with NPs for 24 h. Jurkat cells were resuspended in 1640 medium containing 0.2 μmol/L staurosporine (STS) for 2 h. The post-apoptotic Jurkat cells were labeled with PKH67 according to the manufacturer's directions. Then, RAW264.7 cells were incubated with PKH67-labelled ACs with a cell ratio of 3:1 (ACs:macrophages) for 1 h. The medium was removed and the cells were rinsed with PBS three times before being fixed with 4% paraformaldehyde for 30 min. Ultimately, DAPI was used to stain the nucleus and the images were photographed with Nikon (Ti-E + A1 MP, Japan) confocal microscope.

2.4.4. Western blotting

100 ng/mL LPS was used to treat macrophages to form activated macrophages in 6-cm dishes and then different NPs were added to co-incubate with activated macrophages for 24 h. The remaining steps were performed as previously described[23].

2.4.5. Autophagy flux detection

The adenoviral labeled with the mRFP-GFP-LC3 was supplied by Hanbio (HB-LP2100001). mRFP-GFP-LC3 adenovirus was used to transfect macrophages at 37 °C to observe autophagy flux in HA@PC@Pita NPs-treated cells. After incubation at 37 °C for 20 h, the levels red fluorescent protein mRFP, green fluorescent protein (GFP) and LC3 fusion protein were observed under CLSM (Leica LAS X).

2.4.6. The colocation of LC3 B, p63 and lipids droplet

HA@PC@Pita NPs were used to treat activated macrophages for 24 h. Cells were then stained with LC3 B/BODIPY 493/503 or p62/BODIPY 493/503. Ultimately, the fluorescence images of cells were photographed by CLSM (Leica LAS X, Weitzlar, Germany).

2.4.7. In vitro anti-inflammatory assay

The assay on macrophages was performed in 24-well plates. After cell adhesion, different NPs were incubated with macrophages for 2 h, followed by stimulating with 100 ng/mL LPS for 24 h. Then, ELISA kits were used to detect the changes of extracellular inflammatory factors.

2.5. Animal experiment method

ApoE$^{-/-}$ mice (6 weeks) and C57BL/6 mice (6 weeks) were supplied by Beijing Weishang Lituo Technology Co., Ltd. (Beijing, China). All animal experiments conform to the Guiding Principles of "Declaration of Helsinki" and have been approved by the Medical Ethics Committee of Hunan University (SYXK-2018-0006).

2.5.1. Pharmacokinetic assay

Serum samples were collected from C57BL/6 mice at 0, 0.5, 1, 2, 4, 8, 12, and 24 h after injection of Ce6, PC@Ce6 NPs and HA@PC@Ce6 NPs (the Ce6 concentration was 5 μg/mL). The fluorescence intensity was monitored by An IVIS spectrum system (Lumina XR, Caliper, USA).

2.5.2. Targeting of the atherosclerotic plaques

ApoE$^{-/-}$ mice (6 weeks) feeding with HFD (40% fat, 40% carbohydrate, 20% protein, and 1.25% cholesterol) for 8 weeks were performed to observe the target ability of different NPs. After administering in tail with of Ce6, PC@Ce6 NPs and HA@PC@Ce6 NPs (the Ce6 concentration was 5 μg/mL) for 12 h, the aortas and major organs from euthanizing atherosclerotic mice were collected after 12 h to detect fluorescence intensity by An IVIS spectrum system.

2.6. *In vivo anti-atherosclerosis study*

2.6.1. *Feeding and treatment programs*

After feeding the *ApoE*$^{-/-}$ mice (6 weeks) with HFD (40% fat, 40% carbohydrate, 20% protein, and 1.25% cholesterol) for 10 weeks, the mice were divided into control (normal diet), model (HFD with saline), PC NPs (HFD with 3.6 mg/kg PC), PC + Pita (HFD with 3.6 mg/kg PC and 0.4 mg/kg Pita) and HA@PC@Pita NPs (HFD with 0.4 mg/kg Pita). The mice were injected *via* i.v.-administration three times a week, the therapeutic effect was monitored after 2 weeks of treatment.

2.6.2. *ORO staining of aorta and histological study of the aortic tissue in ApoE*$^{-/-}$ *mice*

Atherosclerotic mice were sacrificed after 2 weeks of treatment. The collected aorta was subjected to ORO staining to observe the change of the plaques. Furthermore, ORO staining on the cryostat section of the aortic root, aortic arch, and aorta abdominals was performed.

The paraffin sections of aortic root were dehydrated for hematoxylin−eosin staining (HE) and Masson staining under the guidance of the kit manual. Immunohistochemistry was developed in the order of restoring the tissues antigens, drowsing peroxidase blocker, avidin, biotin, and adding to antibody incubation overnight. The secondary antibody was then incubated with sections of aortic root, followed by performing color reaction. Ultimately, the sections with sealing in neutral resin were observed under microscope (Olympus, IX-73).

2.7. *Statistical analysis*

GraphPad Prism 8.0 software (GraphPad, USA) with one-way ANOVA was used to analyze data to compare statistical significance of two independent groups. The data were considered as statistical significance if $^{*}P < 0.05$, and all data are presented as the mean ± standard deviation (SD).

3. Results and discussion

3.1. *Fabrication and characterization of HA@PC@Pita NPs*

The preparation scheme of HA@PC@Pita NPs was presented in Fig. 1A. Firstly, we synthesized PC NPs, Supporting Information Fig. S1A visually showed the homogenous PC solution and colloid PC solution after adding glycine and formaldehyde, the result of which reflected the formation of PC NPs through self-assembly. The minimal particle size of PC NPs (size = 217.6 nm) was obtained at the presence of 10 mg/mL glycine and 10 μL of 37% formaldehyde (Fig. S1B). Meanwhile, the minimal polydispersity index of PC NPs (PDI = 0.146) was obtained at 800 rpm (Fig. S1C). UV−Vis spectra indicated that the absorption peak of sole PC at 278 nm bathochromically shifted to 280 nm for PC NPs (Fig. S1D) due to the $\pi-\pi$ stacking of resorcinol in the forming process and molecular length extension of polyphenol oligomers[19]. FT-IR revealed the absorption peak at 1234 cm^{-1} due to the asymmetric stretching vibration of C−O−C in the oxazine ring, the absorption peak at 1323 cm^{-1} due to the rocking vibration of CH_2 in the oxazine ring, while the absorption peak observed at 1736 cm^{-1} due to the stretching vibration of the ester carbonyl C═O in the PC NPs, and the signal peaks of O−H and N−H asymmetric stretching vibrations on the polyether skeleton appeared at 928 cm^{-1} (Fig. S1E). Then, we investigated the effect of solvents on the solubility of PC NPs in order to achieve the ideal loading efficiency of Pita. Fig. S1F indicated that PC NPs efficiently dissolved in DMSO. Taking the above characteristic, PC NPs achieved efficient loading of Pita through solvent conversion. Next, we investigated the effect of PC NPs/Pita ratio and time on the NPs formation and found that PC@Pita NPs with the smallest particle size was obtained for 2 h reassembly with the mass ratio of PC NPs:Pita for 3:0.2 (Fig. S1G and S1H). By combining the standard curve of absorption value of Pita V (Fig. S1I) and the absorption peak (Fig. S1I), the EE and LE of PC NPs loaded with Pita were calculated to be 97.12% and 6.45% respectively (Fig. 1B). In addition, HA modification increased the size of PC@Pita NPs. And the smallest size (146 nm) of HA@PC@Pita NPs was obtained at the NPs/HA ratio of 60: 1 (Fig. S1J). DLS analysis indicated the size and the ζ-potential of HA@PC@Pita NPs for 146 ± 20 nm and −24.2 ± 1.5 mV, respectively (Fig. 1C and D). EDS spectra demonstrated the uniform distributions of C, O, and F in PC and PC@Pita NPs (Fig. 1E), indicating the successful preparation of PC@Pita NPs. The TEM images exhibited the uniformly dispersed spherical shape of all NPs. Among them, PC NPs showed a core−shell structure, while PC@Pita NPs showed spherical shape after filling Pita in the core of PC NPs. Moreover, HA was found in the outside of HA@PC@Pita NPs (Fig. 1F). To further verify the core−shell structure of HA@PC@Pita NPs, fluorophores of Dil and DiO were applied to label PC NPs and pita, respectively. Then, the double fluorophores-labeled PC NPs were co-incubated with macrophages and activated macrophages, as previously reported[24]. The fluorescence images showed the overlapping of red signal (representing the shell of HA@PC NPs) with green signal (representing the core of Pita), indicating a complete "core shell" structure even after internalization into cells (Supporting Information Fig. S2A). Moreover, by comparing the release behavior of HA@PC@Pita NPs under different pH conditions, we found that the release rate at pH 5.4 (slightly acid environment) was faster than that of pH 7.4 (neutral environment) (Fig. 1G). Meanwhile, the produced fragments confirmed the depolymerization of NPs caused by drug release (Fig. 1H). In addition, Fig. 1I demonstrates homogeneous stability as the investigated NPs maintained particle size at 146 ± 26.2 nm for up to 7 days in PBS and 10% FBS solution at 37 °C and pH 7.4. These results provide the possibility for the practical application of HA@PC@Pita NPs.

3.2. *Target ability and therapeutic effect of HA@PC@Pita NPs in vitro*

To investigate the effect of HA modification on the targeting ability of self-assembled NPs, Ce6 loaded NPs were used to track their cellular behavior *in vitro* as previously described[25]. At first, a plaque environment of atherosclerosis was constructed by culturing LPS-treated macrophages with defective efferocytosis in the 24-well plate and HUVECs on the top chamber (Fig. 2A)[26]. Then, we performed Transwell assay to investigate the effect of HA@PC@Ce6 NPs on the efferocytosis of LPS-treated macrophages by directly detecting the uptake ability of NPs. As we expected, the intensity of red fluorescence signal in activated macrophages was significantly higher than that of HUVECs. Moreover, the total red fluorescence intensity in the HA@PC@Ce6-treated activated macrophages was higher than that of PC@Ce6 treated cells (Fig. 2B and C). As the efficient uptake of the activated macrophages to HA@PC@Ce6 NPs can contribute to the CD44-mediated endocytosis[22], we found that HA

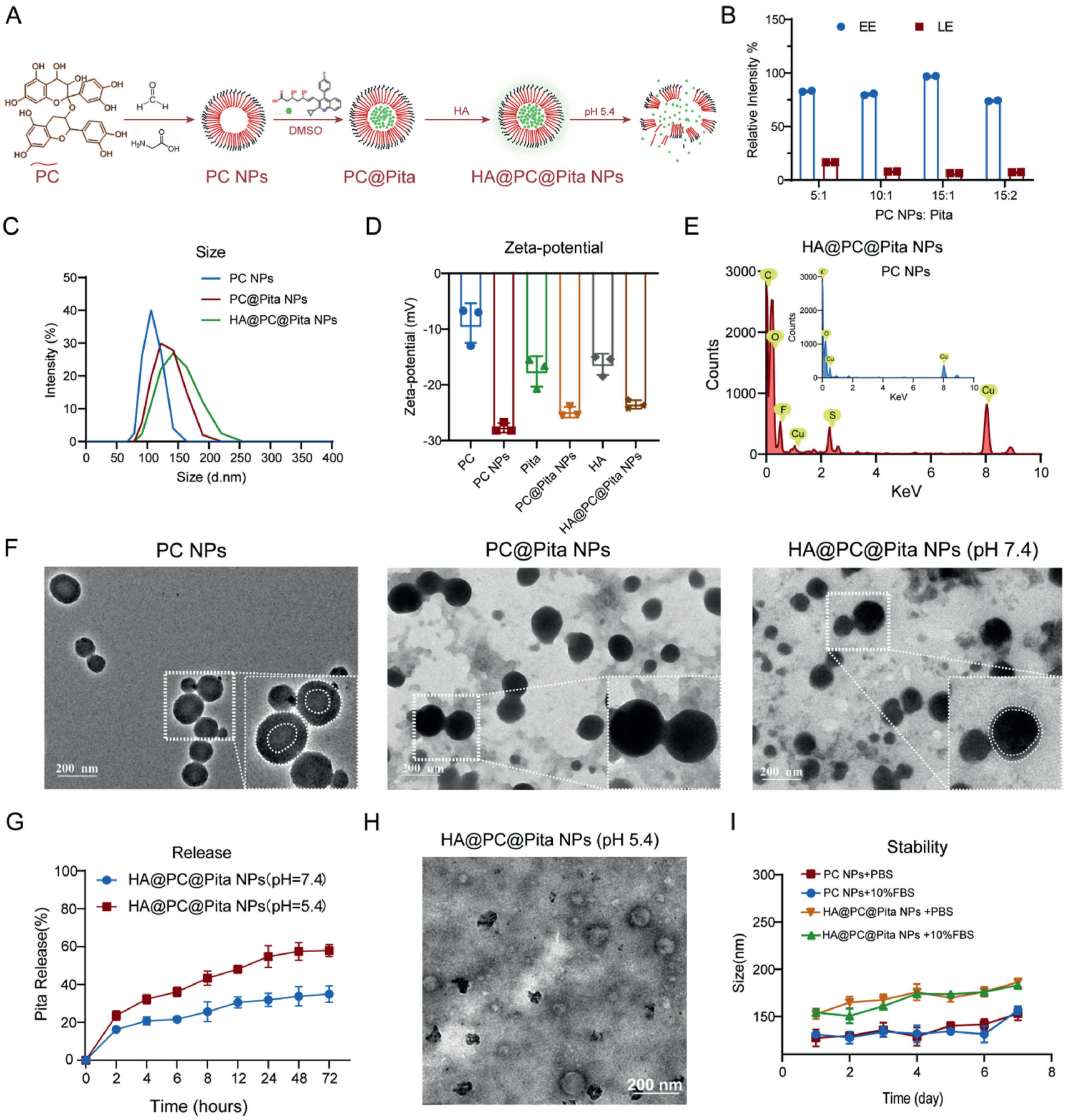

Figure 1 Fabrication and characterization of HA@PC@Pita NPs. (A) Preparation scheme of HA@PC@Pita NPs. (B) Entrapment and loading capacity of Pita. (C) Size of PC NPs, PC@Pita NPs, and HA@PC@Pita NPs. (D) Zeta potentials of PC NPs, PC@Pita NPs, HA@PC@Pita NPs. (E) EDS spectra of PC NPs and HA@PC@Pita NPs. (F) TEM images of PC NPs, PC@Pita NPs, and HA@PC@Pita NPs (pH 7.4). (G) The cumulative release of Pita at different pH values (7.4 and 5.4) at room temperature. (H) TEM image of HA@PC@Pita NPs (pH 5.4). (I) PC NPs and HA@PC@Pita NPs stability assay. The size changes of PC NPs and HA@PC@Pita NPs in the PBS and 10% FBS were monitored for 7 days at room temperature.

pretreatment significantly reduced the red fluorescence signal in HA@PC@Ce6 treated macrophages (Fig. 2D and E). In another experiment, we investigated the effect of HA modification on the immune escape ability of self-assembled NPs from macrophages. Consistent with previous report[27], the red signal in HA@PC@Ce6-treated macrophages was weaker than that of PC@Ce6-treated macrophages, indicating that HA endows NPs with a certain immune escape ability (Supporting Information Fig. S3A and S3B). Moreover, the inhibitors test showed that the signal in activated macrophages with methyl-β-cyclodextrin (vesicle-mediated endocytosis), chlorpromazine (clathrin-mediated endocytosis), and colchicine (macropinocytosis) pretreatment decreased by 62.06%, 57.39%, and 24.5%, respectively (Fig. S3C and S3D). These results indicate that the uptake of HA@PC@Pita NPs by activated macrophage mainly depends on the vesicle-mediated endocytosis and clathrin-mediated endocytosis[28].

Activated macrophages were used to assess the efficacy of HA@PC@Pita NPs on efferocytosis, the process tightly related to the development of atherosclerosis[29]. At first, ORO staining method was used to evaluate the effect of Pita concentration on the foam cell formation. Consistent with previous report[30], ORO signal, which represented ox-LDL in cell, gradually decreased in a Pita concentration dependent manner. 0.2 μmol/L Pita showed the strongest inhibitory effect in foam cell inhibition (Fig. 2F and G). This optimal concentration was adopted for HA@PC@Pita NPs preparation. According to the loading rate of Pita in HA@PC@Pita NPs, the concentration of PC in the NPs was calculated as 2.4 μmol/L. Both of confocal microscopy imaging

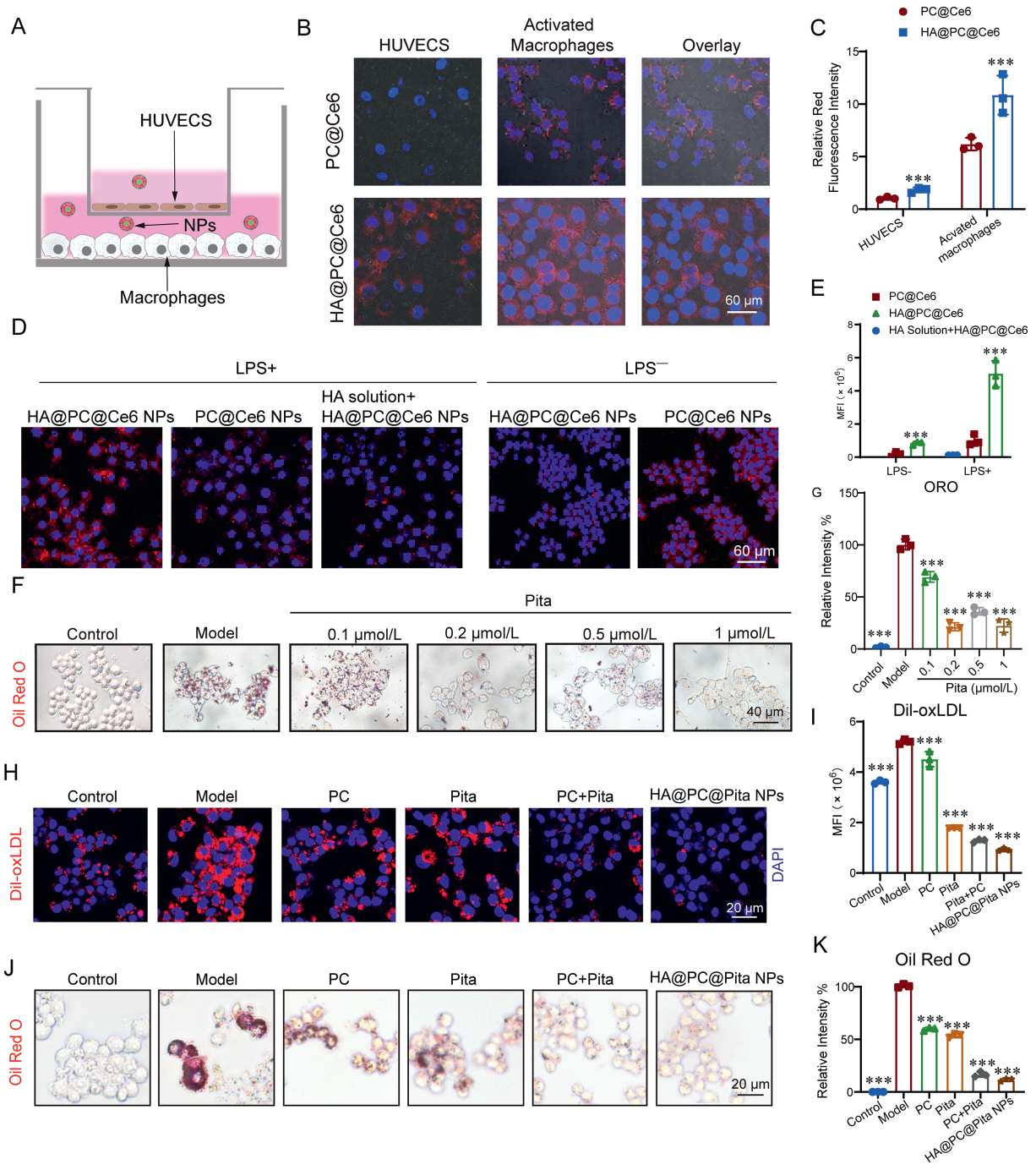

Figure 2 *In vitro* uptake and therapeutic effects of HA@PC@Pita NPs to activated macrophages. (A) A schematic diagram of the transwell assay. (B) Fluorescent images of PC@Ce6 and HA@PC@Ce6 NPs in HUVECs and activated macrophages. (C) Quantitative analysis of fluorescence intensity corresponded to (B). (D, E) CLSM images and quantification analysis of RAW264.7 cells incubated with PC@Ce6 NPs and HA@PC@Ce6 NPs for 4 h after activation by LPS or not. Activated macrophages were pretreated with HA solution (500 μg/mL) and HA@PC@Ce6 NPs (middle column) (scale bars = 60 μm). Cell nuclei were stained by DAPI. (F, G) Optical microscopy images and semi-quantitative analysis of ORO staining in RAW264.7 cells with different concentrations of Pita treatment for 24 h, scale bar = 40 μm. (H, I) CLSM images and semi-quantitative analysis of DiI-oxLDL internalization in RAW264.7 cells. (J, K) Optical microscopy images and semi-quantitative analysis of ORO staining in RAW264.7 cells with different NPs treatment for 24 h, scale bar = 20 μm. Data are presented as mean ± SD ($n = 3$). *$P < 0.05$, **$P < 0.01$, and ***$P < 0.001$. ns, no significant difference.

and ORO staining indicated the strongest inhibitory effect of HA@PC@Pita NPs on the ox-LDL internalization of activated macrophages, which was reflected by the weakest red fluorescence and red signal (Fig. 2H–K). These results demonstrate that HA@PC@Pita NPs can effectively inhibit foam cell formation by reducing oxLDL internalization.

3.3. *HA@PC@Pita NPs repair efferocytosis via regulating M1/M2-type repolarization*

It was reported that Pita could restore efferocytosis by regulating the ERK5/Mertk signaling pathway-mediated macrophage repolarization[31]. By performing immunofluorescence staining of CD206 and CD80 proteins, two markers for M2 and M1 macrophages, respectively, it was found that HA@PC@Pita NPs caused contrary changes for them in activated macrophages (Fig. 3A). Flow cytometry assay indicated that the percentage of M2 ($CD206^+$ cells) and M1 ($CD80^+$ cells) were 61.3% and 21.6%, respectively, in activated macrophages with HA@PC@Pita NPs treatment (Fig. 3B). Western blot assay indicated that HA@PC@Pita NPs significantly upregulated the levels of ERK5, while downregulated p-ERK5 levels with the function of anti-inflammatory and anti-apoptotic in activated macrophages (Fig. 3C). Moreover, re-polarization of macrophages caused by HA@PC@ Pita NPs directly upregulated the levels of Mertk, the

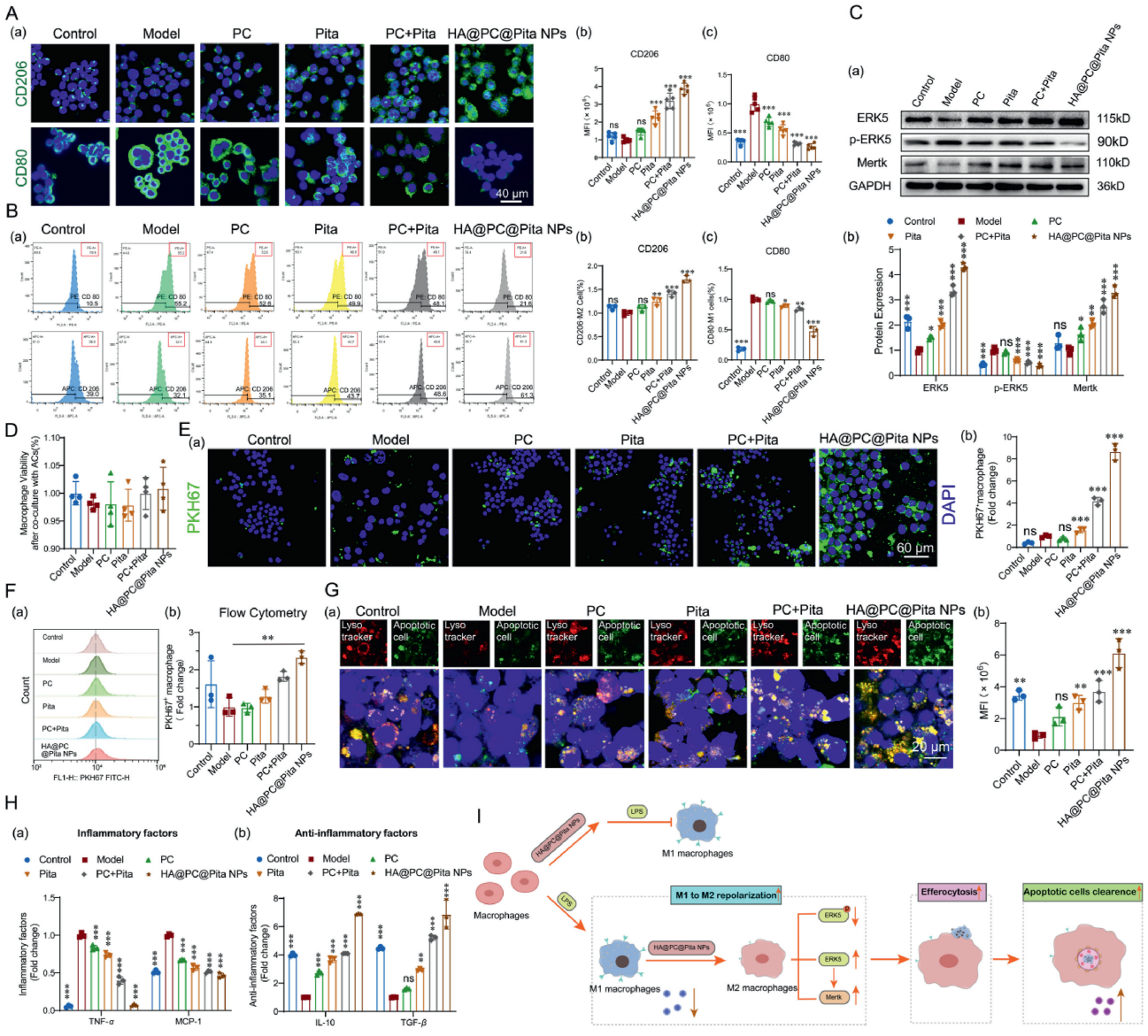

Figure 3 HA@PC@Pita NPs repair efferocytosis *via* regulating M1/M2-type polarization. (A) Immunofluorescence staining (a) and quantitative analysis (b, c) of CD80 (green) and CD206 (green) on macrophages with different treatments, scale bar = 40 μm. (B) Flow cytometry profiles of CD80 highly expressed M1 phenotype and CD206 highly expressed M2 phenotype. (C) Western blot assay (a) and semi-quantitative analysis (b) of ERK5, p-ERK5 and Mertk. (D) Viability assay of HA@PC@Pita NPs treated macrophage after co-culturing with ACs. (E) CLSM images (a) and semi-quantitative analysis (b) of the effect of HA@PC@Pita NPs on the macrophages efferocytosis, scale bar = 60 μm. (F) Intracellular apoptotic cell detection by flow cytometry analysis in macrophages treated with LPS (100 ng/mL). (G) Confocal fluorescence images (a) and semi-quantitative analysis (b) of apoptotic cell elimination by macrophages through lysosomes, scale bar = 20 μm (H) ELISA assay of inflammatory factors (a) and anti-inflammatory factors (b). (I) Mechanism diagram of HA@PC@Pita NPs induced efferocytosis reactivation through skewing pro-inflammatory M1 to pro-efferocytosis M2. [LPS] = 100 ng/mL, [PC] = 2.4 μmol/L, [Pita] = 0.2 μmol/L, n = 3 per treatment, $^*P < 0.05$, $^{**}P < 0.01$, and $^{***}P < 0.001$. ns, no significant difference.

downstream effector of ERK5[32]. As the clearance of ACs by macrophages plays a crucial role in the atherosclerotic lesion development and necrotic core formation[33], we then investigated the effect of HA@PC@Pita NPs on the ACs clearance as previously described[34]. MTT assay first demonstrated negligible viability change of NPs-treated macrophages after co-culturing with ACs (Fig. 3D). Then, activated macrophages incubating with HA@PC@Pita NPs for 24 h were used to culture with PKH67-labeled ACs for 2 h. Fig. 3E and G indicated that the ACs were largely eliminated through lysosomes of macrophages treatment with HA@PC@Pita NPs. This result demonstrated the efferocytosis reactivation function of HA@PC@Pita NPs on activated macrophages. Flow cytometry analysis directly indicated the increased fluorescence signal, which reflected the efferocytosis reactivation of macrophages caused by HA@PC@Pita NPs (Fig. 3F). ELISA assay further indicated the inhibition of HA@PC@Pita NPs on the levels TNF-α and MCP-1 secreted by macrophages, the two factors of TNF-α and MCP-1 upregulating the key "Don't Eat-Me" ligand CD47 on the surface of ACs[35]. In contrast, the degradation of ACs in macrophages through continuous efferocytosis gradually increased the levels of IL-10 and TGF-β (Fig. 3H). From these results, we conclude that HA@PC@Pita NPs can induce high levels of efferocytosis by efficiently re-polarizing macrophages from M1 to M2 type, which finally result in the elimination of ACs clearance in macrophages through ERK5/Mertk pathway (Fig. 3I). However, the effect of residual oxLDL produced by ACs ablation on the phenotype of macrophages should be deeply investigated.

3.4. HA@PC@Pita NPs promote cholesterol efflux through enhancing lipophagy

Through efferocytosis, phagocytes including M2 macrophages can protect the surrounding tissues from the damage of cellular contents such as ox-LDL[36]. Thus, enhancing cholesterol efflux is crucial for avoiding the impairment of excess oxLDL and maintaining normal efferocytosis of macrophages. Meanwhile, normal efferocytosis-related autophagy of macrophages was reported to enhance atherosclerotic plaque stability[37]. In the previous study, we and others have demonstrated that normal autophagy can promote ABCA1/G1-mediated cholesterol efflux to alleviate As[27]. By performing immunofluorescence imaging (Supporting Information Fig. S4A and S4B) and Western blot assay (Fig. 4A and B), we found that autophagy marker protein of LC3 B and cholesterol efflux regulators of ABCG1 and ABCG1 increased 3.5-fold to 4-foldfold in LPS-treated macrophages after treatment with HA@PC@Pita NPs for 24 h. Moreover, colocalization images of the lipid droplet and lysosome indicated that the colocalization part of HA@PC@Pita NPs group is stronger than that of PC group due to the increased bioavailability of self-assemble NPs[38] (Fig. S4C and S4D). Recent studies have shown that cholesterol efflux is closely related to lipophagy[10]. Hence, we detected lipophagy by transfecting activated macrophages with mRFP-GFP-LC3 labeled adenovirus as previously described. The yellow dots (the overlapping of red and green fluorescence) and the red dots in acidic environments represent autophagosomes and autophagosomes[39], respectively. Fig. 4C and D indicated a significant increase of yellow dots in the HA@PC@Pita NPs-treated cells, which reflected the promotion of autophagosomes formation and recovery of autophagic flux. Accordingly, the increase of p62 degradation was found in the same group (Fig. 4E and F), due to the normal fusion of autophagosomes and lysosomes. In another control experiment, using 3-MA, an early autophagy inhibitor[40], to restrain autophagy flux, we found that co-treatment of mRFP-GFP-LC3 labeled adenovirus with 3-MA enhanced red dot number and upregulated p62 levels. Meanwhile, sole 3-MA (1 μmol/L) showed negligible effect on the viability of all macrophages (Fig. S4E). In summary, HA@PC@Pita NPs-induced lipophagy contributes to the recovery of autophagosome-lysosome formation in macrophages.

Increasing evidences have suggested selective activation of lipophagy of atherogenic lipoproteins (ox-LDL and aggregated ox-LDL) in macrophages[9]. Here, the co-localization imaging indicated that HA@PC@Pita NPs treatment increased the co-localization of LDs with LC3 B, while decreased the co-localization of LDs with p62, compared with 3-MA + HA@PC@Pita NPs treatment group (Fig. 4G–I). Moreover, fluorescence imaging indicated that HA@PC@Pita NPs significantly decreased the cellular oil droplets in activated macrophages, which was reversed by 3-MA pretreatment (Fig. 4J and K). Above results indicate that HA@PC@Pita NPs can effectively restrain macrophage foaming by restoring efferocytosis and enhancing lipophagy (Fig. 4L).

3.5. In vivo pharmacokinetic and target behavior of HA@PC@Pita NPs

ApoE$^{-/-}$ mice (6 weeks old) feeding with 2-month HFD were used to investigate the targeting ability of HA@PC@Ce6 NPs to the plaques. Firstly, we investigated the effect of HA on the half-life of NPs. Fig. 5A and B indicated the longer half-life of HA@PC@Ce6 relative to PC@Ce6 NPs (1.001 *vs.* 0.7552). Moreover, a relatively high fluorescence signal appeared in the plaques of the aortic arch and abdominal aorta of mice with HA@PC@Ce6 NPs administration for 12 h, while only weak fluorescence was observed in the similar areas after PC@Ce6 treatment (Fig. 5C and D). This result suggested that HA@PC NPs could more efficiently localize and accumulate in the plaques. Meanwhile, lower fluorescence signal intensities were found in the liver and kidney of mice with HA@PC NPs administration, compared to the mice with PC@Ce6 NPs treatment (Fig. 5E and F). These results demonstrate that HA modification is beneficial for attenuating liver/kidney accumulation and thus increasing the accumulation of HA@PC@Ce6 NPs in the plaques.

3.6. In vivo therapeutic effect on atherosclerosis of HA@PC@Pita NPs

ApoE$^{-/-}$ mice were adopted to prepare advanced atherosclerosis model by feeding 2-month HFD. Then, the mice were used to assess the therapeutic efficacy of HA@PC@Pita NPs. The whole process was indicated as Fig. 6A. In this regimen, the entire aortas of mice fed with HFD for 2 months and treated with NPs for 2 weeks were excised for imaging. Fig. 6B indicated that the NPs treatment differently reduced atherosclerotic lesion area in the enface sample of the aorta, comparing with model. ORO staining of the aorta revealed the strongest anti-atherosclerosis effect of HA@PC@Pita NPs (Supporting Information Fig. S5A and S5B), which was reflected by the significant decrease of the ratio of the plaque area to total aortic area. Decreased lesion area was also noted in histological cross sections at the aortic valve area in HA@PC@Pita NPs group, comparing with model group (Fig. 6C and D). Above results show that HA@PC@Pita NPs can significantly alleviate advanced atherosclerosis.

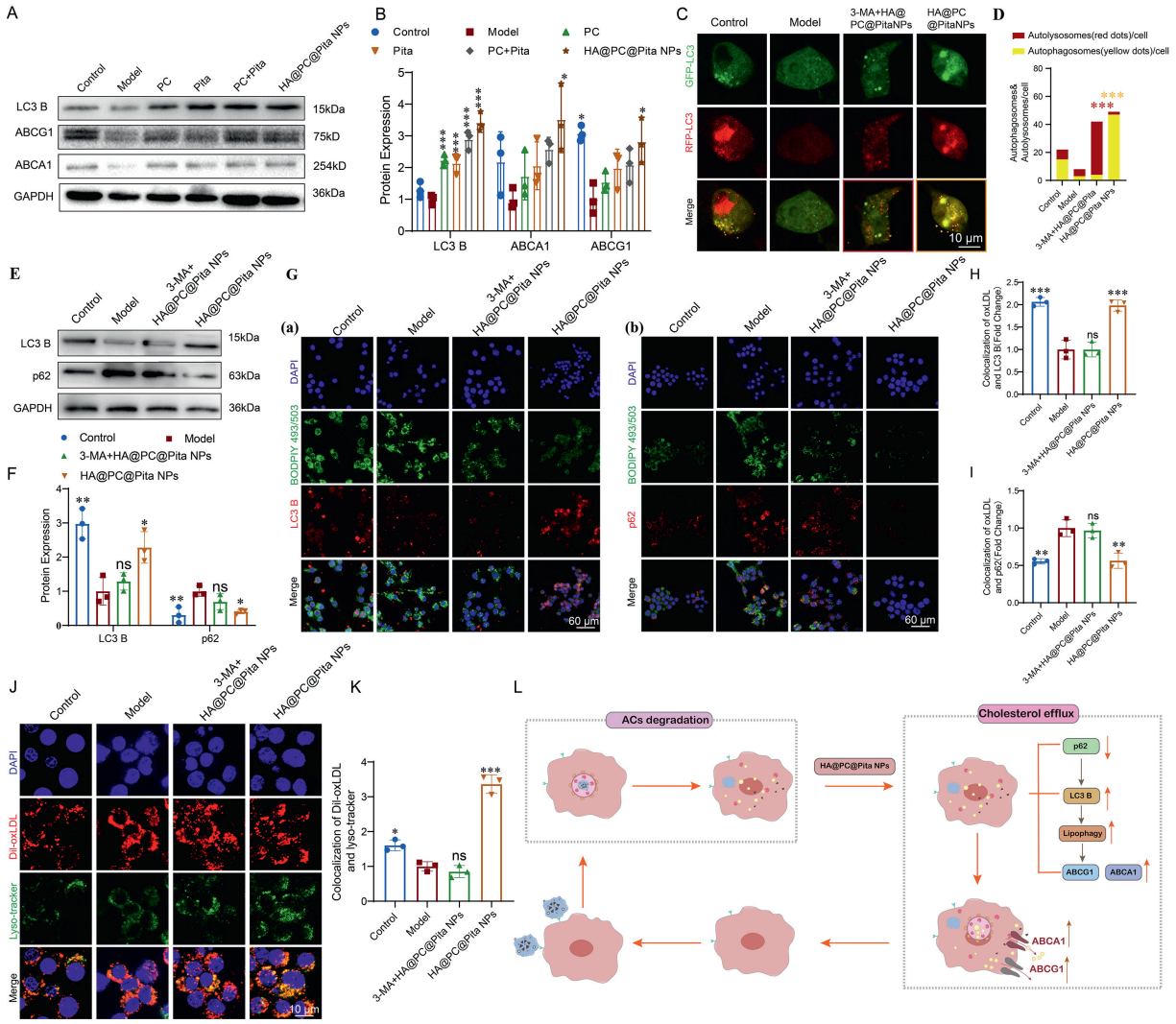

Figure 4 HA@PC@Pita NPs promote cholesterol efflux by regulating lipophagy. (A, B) Western blot analysis and semi-quantitative analysis of LC3 B, ABCA1 and ABCG1. (C, D) CLSM images and quantitative analysis of mRFP-GFP-LC3 levels in macrophages after with different treatments for 20 h. (E, F) Western blot and quantitative analysis of LC3 B and p62 levels in macrophages with different treatments. (G–I) CLSM images and quantitative analysis of co-localization of lipids (green), LC3B (red) and p62 (red). (J, K) CLSM images and quantitative analysis of co-localization of lipids (red) and lysosome (green). (L) Mechanism diagram of HA@PC@Pita NPs promoting cholesterol efflux *via* enhancing lipophagy. [LPS] = 100 ng/mL, [PC] = 2.4 μmol/L, [Pita] = 0.2 μmol/L, $n = 3$ per treatment, $^{*}P < 0.05$, $^{**}P < 0.01$, and $^{***}P < 0.001$. ns, no significant difference.

Advanced atherosclerotic plaque is characterized by the formation of necrotic core[29]. H&E staining clearly illustrated that HA@PC@Pita NPs significantly reduced the lipid-enrichment necrotic core in the aortic root plaque, comparing with model group (Fig. 6E and F). Masson staining revealed that same administration significantly increased collagen deposition surrounding the plaques of mice, which was reflected by the higher positive staining area in this group (indicated by the blue color), compared with the model group (43.7 ± 4.3% *vs.* 19.7 ± 3.5%, $P < 0.05$) (Fig. 6G and H). In addition, immunohistochemistry assay indicated that HA@PC@Pita NPs significantly reduced the levels of MMP-9 and α-SMA in aortic sinus sections (Fig. 6I–L). It was reported that the high levels of MMP-9 and α-SMA can contribute to the rupture of atherosclerotic plaques and lead to myocardial infarction and stroke, even death[41]. In turn, the thick fibrous cap caused by collagen deposition and low levels of MMP secretion in plaques can reduce the risk for rupture[42]. Therefore, we can suspect that HA@PC@Pita NPs can prevent emergency medical conditions by reducing atherosclerotic plaque size and preventing the rupture of plaques. Moreover, immunohistochemistry staining with anti-CD31 antibody (HUVECs marker) revealed that HA@PC@Pita NPs effectively reduced the number of $CD31^{+}$ new vessel in the atherosclerotic plaque region (Fig. 6M and N), which is beneficial for reducing the vulnerable plaques caused by the large brittle rupture of the rich vascular network. Above results indicate that HA@PC@Pita NPs effectively inhibit atherosclerotic plaques development and increase plaque stability, as well.

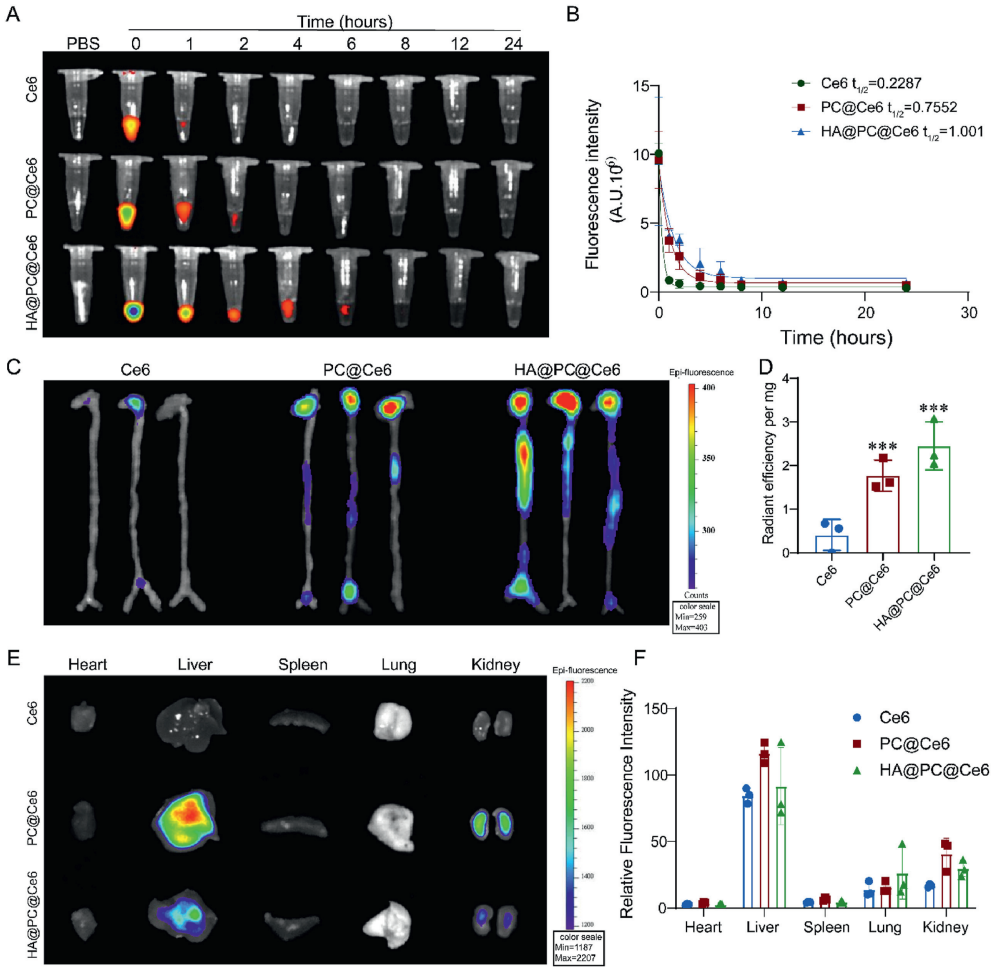

Figure 5 *In vivo* circulation and targeting capability assay of HA@PC@Pita NPs. (A, B) Fluorescence images and pharmacokinetic curves of Ce6, PC@Ce6 and HA@PC@Ce6 in the blood at different time points. (C, D) The fluorescence images and quantitative analysis of the aorta of *ApoE*$^{-/-}$ mice. (E, F) The fluorescence images and quantitative analysis of the major organs excised from the *ApoE*$^{-/-}$ mice with different administrations. Data are mean ± SD ($n = 3$), *$P < 0.05$, **$P < 0.01$, ***$P < 0.001$ *vs*. the PC@Ce6 group. ns, no significant difference.

3.7. In vivo anti-atherosclerosis mechanism of HA@PC@Pita NPs

The proinflammatory microenvironment of plaques can inhibit the expression of key efferocytosis molecules ERK5/Mertk[31]. In turn, high expression of ERK5 can restore efferocytosis *via* upregulating Mertk levels in M2 phenotype macrophages[6]. Significant decrease in the CD80-positive proportion (M1 marker) and elevation in the CD206-positive proportion (M2 marker) were observed in HA@PC@Pita NPs treated macrophages (Fig. 7A and B), indicating the reduction of M1-phenotype macrophages involved in lipid accumulation and increase of M2-phenotype macrophages involved in inflammatory ablation and plaque stabilization[31]. Immunohistochemistry assay also indicated significant increase of ERK5 and Mertk levels in the same group (Fig. 7C and D). As long-term accumulation of ACs caused by defective efferocytosis is closely related to the plaque formation and atherosclerosis severity[2], we then detected the macrophage phagocytic index of the valve by investigating the co-localization of macrophages and ACs. As shown in Fig. 7E and F, the significant ratio increase of macrophage-engulfed ACs to free ACs and the number decrease of caspases-3 positive ACs suggested enhancement of efferocytosis in the HA@PC@Pita NPs group. Moreover, the mice with HA@PC@Pita NPs treatment exhibited the lowest tunnel positive cells in the plaques among these groups (Fig. 7G and H), which reflected the efficient clearance of ACs by macrophages. Meanwhile, ELISA assay indicated that HA@PC@Pita NPs decreased the levels of MCP-1 and TNF-α, while upregulated the levels of IL-10 in serum. In contrast, apoptotic cell accumulation in advanced lesions resulted in the upregulation of MCP-1 and TNF-α, compared with the normal group (Fig. 7I and J). Overall, the efficient anti-atherosclerotic effect elicited by HA@PC@Pita NPs can attribute to the repolarization of M1 to M2 macrophage and efferocytosis restoration through the ERK5/Mertk pathway.

In addition, several methods were adopted to investigate the effect of HA@PC@Pita NPs on lipophagy of macrophages in plaques. Immunofluorescence staining indicated the upregulation of LC3B levels and the decrease of p62 levels (by 1.7-fold) caused by HA@PC@Pita NPs administration (Fig. 8A and B). Meanwhile, the high yellow signal in Fig. 8C and D reflected the co-localization increase of LAMP1 (a lipophagy marker)[43] and

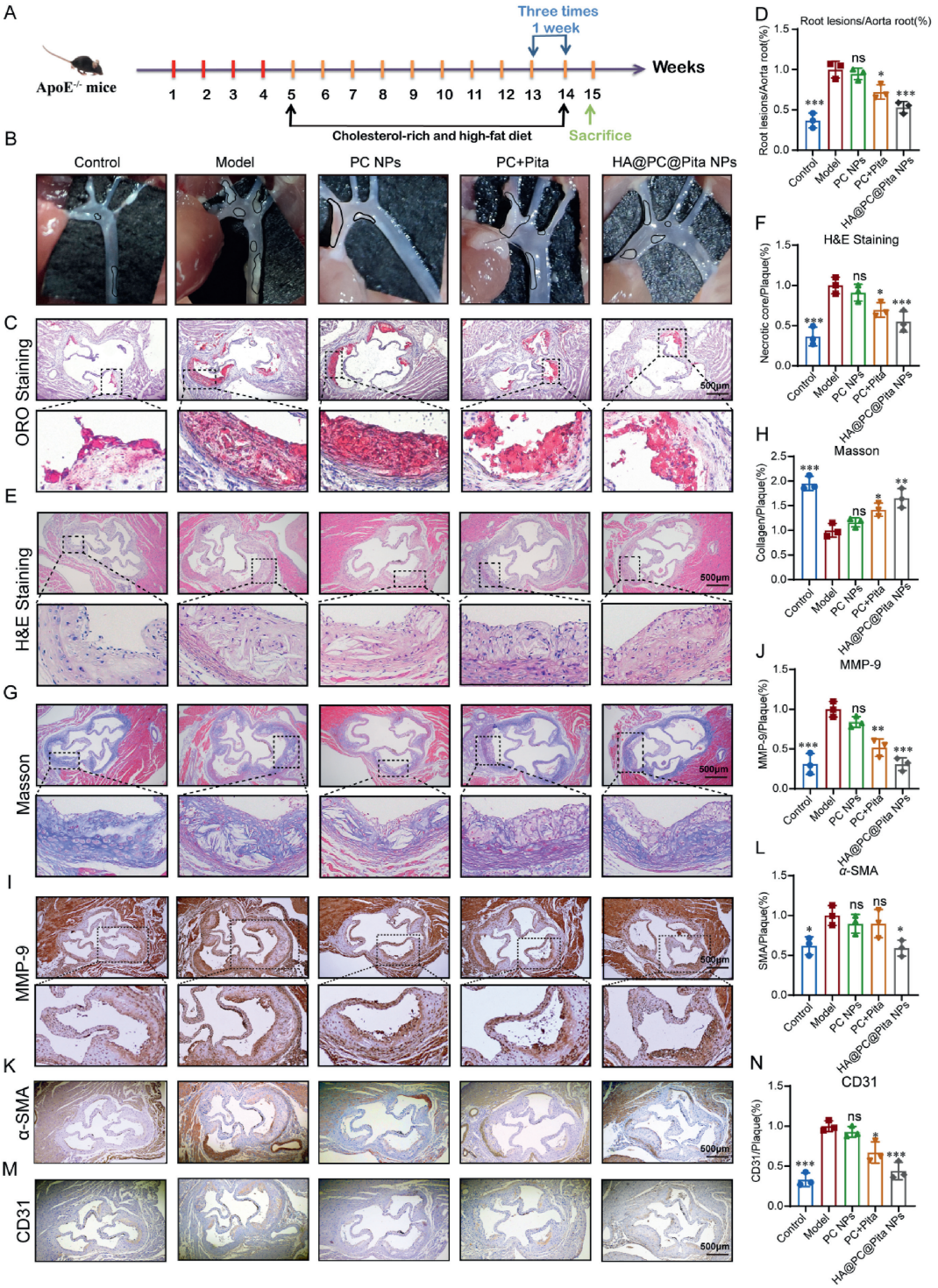

Figure 6 Therapeutic efficacy of HA@PC@Pita NPs in *ApoE*$^{-/-}$ mice. (A) Schematic diagram of treatment process. (B) Representative images depict the entire aortic arch. (C, D) ORO staining and quantitative analysis of aortic root. (E−N) Representative images and quantitative analysis of aortic root sections stained with H&E, Masson's trichrome, anti-MMP-9, anti-α-SMA, anti-CD31. Scale bar = 500 μm. Data are mean ± SD (n = 3), *$P < 0.05$, **$P < 0.01$, ***$P < 0.001$ *vs*. the Model. ns, no significant difference.

lipid droplets at plaques of mice with same administration. Moreover, HA@PC@Pita NPs significantly upregulated the levels of ABCA1/G1 proteins (Fig. 8E and F).

As reported, HDL helps remove cholesterol in circulation by carrying cholesterol back to the liver for disposal and excretion through bile[44]. Upregulating of ABCA1 and ABCG1 in liver enhances lipid metabolism capacity, continuously removes ox-LDL in advanced atherosclerosis circulation, suppresses the progression of advanced atherosclerosis, and stabilizes advanced plaques[45]. As shown in Supporting Information Fig. S6A and S6B, the levels of

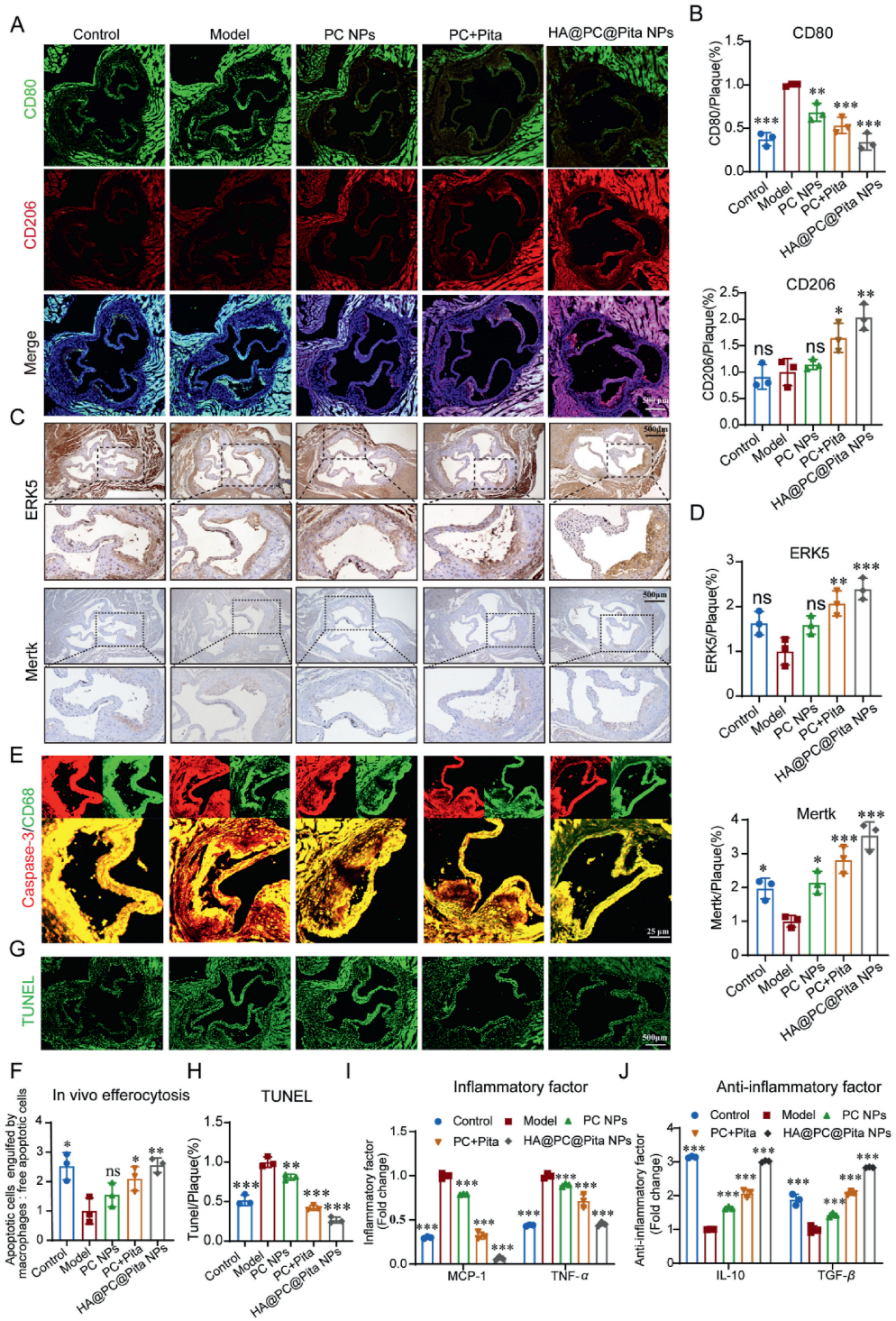

Figure 7 Efferocytosis restoration of *ApoE*$^{-/-}$ mice with HA@PC@Pita NPs treatment. (A, B) Representative immunofluorescence staining images and semi-quantitative analysis of CD80 (green) and CD206 (red). (C, D) Representative immunohistochemistry staining images and semi-quantitative analysis of levels of ERK5 and Mertk. (E−H) Representative immunofluorescence staining images and semi-quantitative analysis of CD68 (green), Caspase-3 (red) and TUNEL (green). (I, J) ELISA analysis of TNF-α, MCP-1, TGF-β and IL-10 levels in serum of mice with different treatments. Data are presented as mean ± SD ($n = 3$). *$P < 0.05$, **$P < 0.01$, and ***$P < 0.001$. ns, not significant.

ABCA1 and ABCG1 were significantly upregulated in the liver of HA@PC@Pita NPs group, indicating that HA@PC@Pita NPs can enhance lipid metabolism capacity of the liver. Above results clearly demonstrate that HA@PC@Pita NPs can promote cholesterol efflux through enhancing lipophagy, simultaneously strengthening lipid metabolism in the liver to alleviate atherosclerosis.

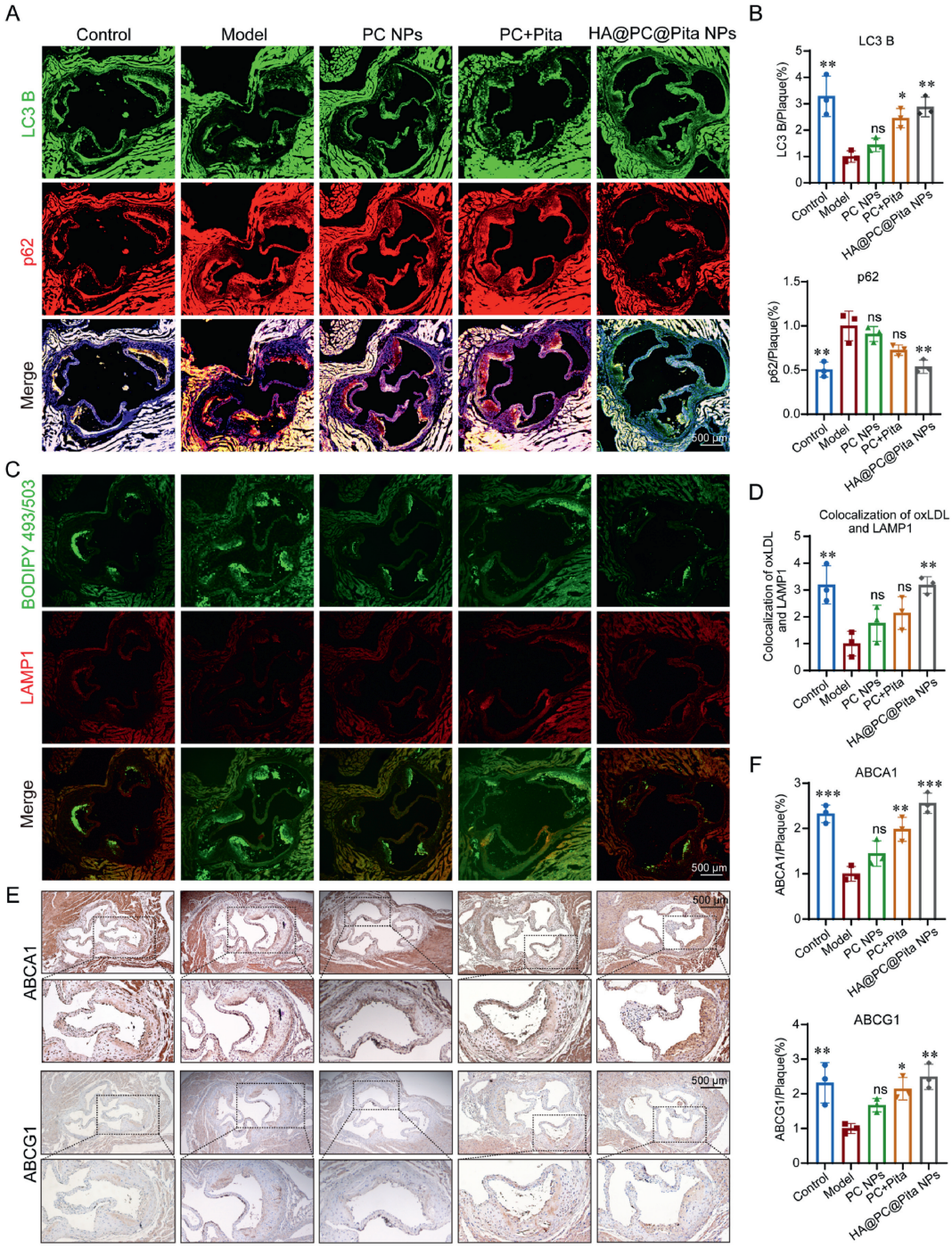

Figure 8 HA@PC@Pita NPs promote lipophagy-mediated macrophages cholesterol efflux *in vivo*. (A, B) Representative immunofluorescence staining images and semi-quantitative analysis of LC3 B (green) and p62 (red) levels. (C, D) Representative immunofluorescence staining images and semi-quantitative analysis of lipid droplets (green) and LAMP1 (red) levels. (E, F) Representative immunohistochemistry staining images and semi-quantitative analysis of ABCA1 and ABCG1 levels in the aortic root. Data are presented as mean ± SD ($n = 3$). *$P < 0.05$, **$P < 0.01$, and ***$P < 0.001$. ns, no significant difference.

3.8. Biocompatibility and biosafety of HA@PC@Pita NPs

Biocompatibility evaluation is crucial to determine the possibility of nanomaterials for clinical application[46]. The cytotoxicity of HA@PC@Pita NPs to different cells was evaluated by MTT assay. Supporting Information Fig. S7A−S7E indicated the high viability of cells after even co-culturing with 80 μg/mL NPs, which suggested the ultra-low cytotoxicity. Using mouse erythrocytes, we performed a homolysis assay. Meanwhle, pure water and PBS were used as the positive and negative controls. As we expected, negligible hemolysis was found for NPs even at a concentration of 80 μg/mL after incubating with blood samples

for 4 h (Fig. S7F and S7H). Moreover, erythrocytes incubated with NPs still showed intact morphology (Fig. S7G). Above results indicate the favorable biocompatibility of HA@PC@Pita NPs for practical application.

In vivo biosafety of nanoparticles was further evaluated *via* i.v.-administration. Comparing with the normal mice, no significant change was found for blood routine indexes and clinical serum biochemical parameters in $ApoE^{-/-}$ mice treated with HA@PC@Pita NPs (Supporting Information Fig. S8A and S8B). In addition, Fig. S8C illustrated the most comparable levels of LDL, HDL, TC, and TG between the normal and HA@PC@Pita NPs group. HE staining of heart, liver, spleen, lung, and kidney proved that i.v.-administration of HA@PC@Pita NPs did not damage these organs including morphological changes or signs of inflammation (Fig. S8D), which was reflected by the ladder-shaped and well-organized myocardial fibers, rows hepatocytes, red and white marrow of the spleen clear alveolar structure, uniform size of glomeruli, normal shape, well defined boundary of kidneys. Above results suggested the high biosafety of i.v.-administration of HA@PC@Pita NPs and the potential for clinical application.

4. Conclusions

In this study, we constructed HA@PC@Pita NPs to simultaneously deliver PC and Pita into macrophages at atherosclerotic plaques. The rationally engineered HA@PC@Pita NPs could alleviate advanced atherosclerosis by restoring macrophage efferocytosis *via* facilitating the M2 polarization and upregulating ERK5/Mertk expression. Meanwhile, HA@PC@Pita NPs could maintain the natural function of the M2 macrophages through promoting macrophage cholesterol efflux *via* enhancing lipophagy. *In vitro* and *in vivo* studies indicated that HA@PC@Pita NPs achieved the admirable effect of clear necrotic core. Therefore, these results demonstrate the application of this universal platform applicable for the treatment of atherosclerosis.

Acknowledgments

This work is supported by the Open Program of NHC Key Laboratory of Metabolic Cardiovascular Diseases Research, Yinchuan, China; the Natural Science Foundation of Hunan Province (2022JJ40698, China); the National Natural Science Foundation of China for Regional Projects (82060264, 82260142); Key Research and Development Projects in Ningxia Province (2018BEG02004, China); The "Phoenix Introduction Plan" Talent Startover Project of The Second Affiliated Hospital of Air Force Medical University (2023YFJH011, China).

Author contributions

Yizhou Wu, Hongyan Zhou and Hao Liu prepared the self-assembled nanoparticles and performed the characterization and cell experiments; Jiayao Hu, Yue Sun, Wei Yan and Chunyi Tong participated in animal experiments; Yizhou Wu wrote the manuscript with contributions from Bin Liu, Ying Kong; Bin Liu provided conceptual advice and revised the manuscript. All the authors contributed to the proofreading and corrections of the manuscript.

Conflicts of interest

The authors declare no conflicts of interest.

Appendix A. Supporting information

Supporting information to this article can be found online at https://doi.org/10.1016/j.apsb.2024.08.006.

References

1. Grover SP, Mackma N. Tissue factor in atherosclerosis and atherothrombosis. *Atherosclerosis* 2020;**307**:80−6.
2. Kojima Y, Weissman IL, Leeper NJ. The role of efferocytosis in atherosclerosis. *Circ* 2017;**135**:476−89.
3. Tajbakhsh A, Gheibihayat SM, Askari H, Savardashtaki A, Pirro M, Johnston TP, et al. Statin-regulated phagocytosis and efferocytosis in physiological and pathological conditions. Pharmacol *Ther* 2022;**238**: 108282−96.
4. Charvet LY, Pagler TA, Seimon TA, Thorp E, Welch CL, Witztum JL, et al. ABCA1 and ABCG1 protect against oxidative stress−induced macrophage apoptosis during efferocytosis. *Circ Res* 2010;**106**:1861−9.
5. Doran AC, Yurdagul A, Tabas I. Efferocytosis in health and disease. *Nat Rev Immunol* 2019;**20**:254−67.
6. Heo KS, Cushman HJ, Akaike M, Woo CH, Wang X, Qiu X, et al. ERK5 activation in macrophages promotes efferocytosis and inhibits atherosclerosis. *Circ* 2014;**130**:180−91.
7. Mehrotra P, Ravichandran KS. Drugging the efferocytosis process: concepts and opportunities. *Nat Rev Drug Discov* 2022;**21**:601−20.
8. Yasuda T, Ishida T, Miyamoto Sasaki M, Monguchi T, Hirata KI. Pitavastatin increases HDL particles with preserved anti-atherosclerotic proferties in dys lipidemic patients. *J Am Coll Cardiol* 2013;**61**:708−16.
9. Laval T, Ouimet M. A role for lipophagy in atherosclerosis. *Nat Rev Cardiol* 2023;**20**:431−2.
10. Wang YM, Tang H, Tang YJ, Liu J, Yin YF, Tang YL, et al. ASIC1/RIP1 accelerates atherosclerosis *via* disrupting lipophagy. *J Adv Res* 2023;**11**:103732−44.
11. Thompson PD, Panza G, Zaleski A, Taylor B. Statin-associated side effects. *J Am Coll Cardiol* 2016;**67**:2395−410.
12. Peters EB, Kibbe MR. Nanomaterials to resolve atherosclerosis. *ACS Biomater Sci Eng* 2020;**6**:3693−712.
13. Chamundeeswari M, Jeslin J, Verma ML. Nanocarriers for drug delivery applications. Environ *Chem Lett* 2019;**17**:849−65.
14. Liu LH, Zhang XZ. Carrier-free nanomedicines for cancer treatment. *Prog Mater Sci* 2022;**125**:100919−76.
15. Tian M, Chen GC, Xu JC, Lin Y, Yi Z, Chen XY, et al. Epigallocatechin gallate-based nanoparticles with reactive oxygen species scavenging property for effective chronic periodontitis treatment. *Chem Eng J* 2022;**433**:132197−212.
16. Chen Z, Liu B, Gong Z, Huang H, Gong Y, Xiao W. Metagenomics Approach to the intestinal microbiome structure and abundance in high-fat-diet-induced hyperlipidemic rat fed with (−)-epigallocatechin-3-gallate nanoparticles. *Molecules* 2022;**27**:4894−914.
17. Basavalingappa V, Guterman T, Tang Y, Nir S, Lei J, Chakraborty P, et al. Expanding the functional scope of the fmoc-diphenylalanine hydrogelator by introducing a rigidifying and chemically active urea backbone modification. *Adv Sci* 2019;**12**:1900218−27.
18. Zhu W, Oteiza PI. NADPH oxidase 1: a target in the capacity of dimeric ECG and EGCG procyanidins to inhibit colorectal cancer cell invasion. *Redox Biol* 2023;**65**:102827−39.
19. Liu C, Wu H, Duan H, Hou Y, Wang S, Liu Y, et al. An EGCG-mediated self-assembled micellar complex acts as a bioactive drug carrier. *Food Chem* 2023;**418**:135939−51.
20. Zhang B, Qin YM, Yang L, Wu Y, Chen NY, Li MY, et al. A polyphenol-network-mediated coating modulates inflammation and vascular healing on vascular stents. *ACS Nano* 2022;**16**:6585−97.

21. Luo SY, Wang Y, Shen SH, Tang P, Liu ZY, Zhang S, et al. IR780-loaded hyaluronic acid@gossypol−Fe(III)−EGCG infinite coordination polymer nanoparticles for highly efficient tumor photothermal/coordinated dual drugs synergistic therapy. *Adv Funct* 2021; **31**:2100954−74.
22. Lee GY, Kim JH, Choi KY, Yoon HY, Kim KM, Kwon IC, et al. Hyaluronic acid nanoparticles for active targeting atherosclerosis. *Biomaterials* 2015;**53**:341−8.
23. Li YL, Yang AN, Sun Y, Liu DY, You PD, Zeng YL, et al. Hydroxysafflor yellow A-loaded biomimetic liposomes alleviate HHcy-induced atherosclerosis by regulating methylation related autophagy. *Mater Des* 2023;**227**:111807−24.
24. Wang Y, Zhang K, Qin X, Li TH, Qiu JH, Yin TY, et al. Biomimetic nanotherapies: red blood cell based core−shell structured nanocomplexes for atherosclerosis management. *Adv Sci* 2019;**6**: 1900172−85.
25. Song JW, Ahn JW, Lee MW, Kim HJ, Kang DO, Kim RH, et al. Targeted theranostic photoactivation on atherosclerosis. *J Nanobiotechnol* 2021;**19**:338−57.
26. Liang X, Li H, Li X, Tian X, Zhang A, Luo Q, et al. Highly sensitive H_2O_2-scavenging nano-bionic system for precise treatment of atherosclerosis. *Acta Pharm Sin B* 2023;**13**:372−89.
27. Zhou HY, You PD, Liu H, Fan JL, Tong CY, Yang AN, et al. Artemisinin and procyanidins loaded multifunctional nanocomplexes alleviate atherosclerosis *via* simultaneously modulating lipid influx and cholesterol efflux. *J Control Release* 2022;**341**:828−43.
28. He W, Xing XY, Wang XL, Wu DR, Wu W, Guo JL, et al. Nanocarrier-mediated cytosolic delivery of biopharmaceuticals. *Adv Funct Mater* 2020;**30**:1910566−88.
29. Flores AM, Hosseini-Nassab N, Jarr KU, Ye JQ, Zhu XJ, Wirka R, et al. Pro-efferocytic nanoparticles are specifically taken up by lesional macrophages and prevent atherosclerosis. *Nat Nanotechnol* 2020;**15**: 154−61.
30. Shunsuke K, Tetsuya M, Soichi N, Kei S, Junichiro K, Kaku N, et al. Nanoparticle-mediated delivery of pitavastatin inhibits atherosclerotic plaque destabilization/rupture in mice by regulating the recruitment of inflammatory monocytes. *Circulation* 2014;**129**: 896−906.
31. Yang H, Liu C, Wu YJ, Yuan M, Huang JR, Xia YH, et al. Atherosclerotic plaque-targeted nanotherapeutics ameliorates atherogenesis by blocking macrophage-driven inflammation. *Nano Today* 2022;**42**. 101351-6.
32. Abe JI, Imanishi M, Li S, Zhang A, Ko KA, Samanthapudi VSK, et al. An ERK5−NRF2 axis mediates senescence-associated stemness and atherosclerosis. *Circ Res* 2023;**133**:25−44.
33. Tao W, Yurdagul AY, Kong N, Li WL, Wang XB, Doran AC, et al. SiRNA nanoparticles targeting CaMKIIγ in lesional macrophages improve atherosclerotic plaque stability in mice. *Sci Transl Med* 2020; **12**:1063−75.
34. Kojima Y, Volkmer JP, McKenna K, Civelek M, Lusis AJ, Miller CL, et al. CD47-blocking antibodies restore phagocytosis and prevent atherosclerosis. *Nature* 2016;**536**:86−90.
35. Tabas I. Macrophage death and defective inflammation resolution in atherosclerosis. *Nat Rev Immunol* 2010;**10**:36−46.
36. Sene A, Khan AA, Cox D, Nakamura REI, Santeford A, Kim BM, et al. Impaired cholesterol efflux in senescent macrophages promotes age-related macular degeneration. *Cell Metab* 2013;**17**:549−61.
37. Shao BZ, Han BZ, Zeng YX, Su DF, Liu C. The roles of macrophage autophagy in atherosclerosis. *Acta Pharmacol Sin* 2016;**37**:150−6.
38. Dai WZ, Ruan CC, Zhang YM, Wang JJ, Han J, Shao ZH, et al. Bioavailability enhancement of EGCG by structural modification and nano-delivery: a review. *J Funct Foods* 2020;**65**:103732−41.
39. Klionsky DJ, Abdelmohsen K, Abe A, Abedin MJ, Abeliovich H, Acevedo Arozena A, et al. Guidelines for the use and interpretation of assays for monitoring autophagy. *Autophagy* 2016;**12**:1−222.
40. Xia Y, Liu N, Xie XX, Bi GY, Ba HP, Li L, et al. The macrophage-specific V-ATPase subunit ATP6V0D2 restricts inflammasome activation and bacterial infection by facilitating autophagosome−lysosome fusion. *Autophagy* 2019;**15**:960−75.
41. Xu H, She PY, Zhao ZY, Ma BX, Li GX, Wang YB. Duplex responsive nanoplatform with cascade targeting for atherosclerosis photoacoustic diagnosis and multichannel combination therapy. *Adv Mater* 2023;**35**:2300439−55.
42. Vergallo R, Crea F. Atherosclerotic plaque disruption and healing. *Eur Heart J* 2020;**41**:4079−80.
43. Jiang L, Zheng H, Lyu QY, Hayashi S, Sato K, Sekido Y, et al. Lysosomal nitric oxide determines transition from autophagy to ferroptosis after exposure to plasma-activated Ringer's lactate. *Redox Biol* 2021;**43**:101989−2001.
44. Sanmarco LM, Wheeler MA, Gutiérrez-Vázquez C, Polonio CM, Linnerbauer M, Pinho-Ribeiro FA, et al. Gut-licensed IFNγ^+ NK cells drive LAMP1$^+$TRAIL$^+$ anti-inflammatory astrocytes. *Nature* 2021; **590**:473−9.
45. Li H, Yu XH, Ou X, Ouyang XP, Tang CK. Hepatic cholesterol transport and its role in non-alcoholic fatty liver disease and atherosclerosis. *Prog Lipid Res* 2021;**83**:101109−35.
46. Xu M, Zhu J, Wang FF, Xiong YJ, Wu YK, Wang QQ, et al. Improved *in vitro* and *in vivo* biocompatibility of graphene oxide through surface modification: poly(acrylic acid) functionalization is superior to PEGylation. *ACS Nano* 2016;**10**:3267−81.